Dependence of nuclear quadrupole resonance transitions on the electric field gradient asymmetry parameter for nuclides with half-integer spins

Herman Cho

Physical and Computational Sciences Directorate, P. O. Box 999, Pacific Northwest National Laboratory, Richland, WA 99352, USA

A B S T R A C T

Allowed transition energies and eigenstate expansions have been calculated and tabulated in numerical form as functions of the electric field gradient asymmetry parameter for the zero field Hamiltonian of quadrupolar nuclides with $I = 3/2, 5/2, 7/2$, and $9/2$. These results are essential to interpret nuclear quadrupole resonance (NQR) spectra and extract accurate values of the electric field gradient tensors. Applications of NQR methods to studies of electronic structure in heavy element systems are proposed.

© 2016 Elsevier Inc. All rights reserved.

Contents

1. Introduction

Nuclear quadrupole resonance (NQR) spectroscopy has long been a vital method for studying electronic structure in condensed matter [1,2] and for performing high resolution measurements of nuclear quadrupole moments [3–5]. The key parameter obtained from NQR measurements is the electric field gradient (EFG) tensor at the nuclear coordinates, which is completely determined by two independent variables, viz., the zz component of the field gradient $V_{zz} \equiv \partial^2 \phi / \partial z^2$ and the tensor's asymmetry parameter $\eta \equiv (V_{xx} - V_{yy})/V_{zz}$ [2,6].

The dependence of NQR transition frequencies and intensities on the EFG tensor has been numerically mapped [7–11]. Values for η and V_{zz} may be estimated from experimentally measured NQR spectra by referring to data from this previous work. However, the approximation methods used in past calculations did not provide accurate or complete results for many cases of interest, and a more advanced and comprehensive analysis is needed for reliable interpretation of experimental spectra, especially for large η and spin quantum numbers I.

Computational formalisms have recently been described that may be used to characterize the dependence of NQR spectra on η and V_{zz} with substantially improved accuracy and detail [12,13]. The methods are generalizable to arbitrary spin quantum number I, but the majority of nuclei that are of interest for NQR spectroscopy have half-integer spin, i.e., $I = 3/2, 5/2, 7/2$, etc., ^{14}N with $I = 1$ being a notable exception. To demonstrate this approach therefore while providing data of greatest value for the interpretation of NQR experiments, quadrupolar nuclides with half-integral spin are considered exclusively in this paper.

2. Computational method

The zero field spin Hamiltonian of a quadrupolar nuclide in the principal axis system (PAS) of the EFG tensor has the form [2,6]

$$\mathcal{H}_Q = \frac{eQV_{zz}}{4I(2I-1)h} \left[3I_z^2 - \mathbf{I}^2 + \eta \left(I_x^2 - I_y^2 \right) \right] \tag{1a}$$

$$= \frac{eQV_{zz}}{4I(2I-1)h} \left[3I_z^2 - \mathbf{I}^2 + \frac{\eta}{2} \left(I_+^2 + I_-^2 \right) \right]. \tag{1b}$$

For $\eta = 0$, this Hamiltonian has the same eigenstates as the operator I_z; we write these states as $|m\rangle$, with m representing the eigenvalues of I_z, $I \geq m \geq -I$. The eigenstates of $\mathcal{H}_Q$ may be expressed more generally as a linear superposition of the basis states with normalized complex coefficients that are functions of η, namely

$$|\psi_n(\eta)\rangle = \sum_{m=-I}^{I} c_{nm}(\eta)|m\rangle, \tag{2}$$

where $|\psi_n(0)\rangle = |n\rangle$. Similarly, the eigenvalue of $\mathcal{H}_Q$ corresponding to the eigenstate $|\psi_n(\eta)\rangle$ can be written as a function of η, i.e., $\lambda_n(\eta)$. Because of the bilinear I_+^2 and I_-^2 terms in Eq. (1b), the only non-zero coefficients in Eq. (2) will be those with $m = n \pm 2q$, q being an integer.

The mixing of states for non-zero η is embodied by the complex coefficients in the summation in Eq. (2), which can be written

$$c_{nk}(\eta) = \langle k|\psi_n(\eta)\rangle, \tag{3}$$

where $|k\rangle$ is an eigenstate of I_z. A quantitative measure of the superposition of $|m\rangle$ states is the magnitude of $c_{nk}(\eta)$, given by the expression

$$|c_{nk}(\eta)| = \left[c_{nk}(\eta) c_{nk}^*(\eta) \right]^{1/2}$$
$$= |\langle k|\psi_n(\eta)\rangle| . \tag{4}$$

Plots of $|\langle k|\psi_n(\eta)\rangle|$ vs. η thus reveal the extent to which variation of η mixes the basis states in the expansion of $|\psi_n(\eta)\rangle$.

To visualize the dependence of the eigenvalues and eigenstates of $\mathcal{H}_Q$ on η, it is necessary to explicitly solve for $|\psi_n(\eta)\rangle$ and $\lambda_n(\eta)$ for a densely spaced array of η values over the allowed range $1 \geq \eta \geq 0$. Evaluation of the eigenvalues is considerably simplified by observing that the matrix form of $\mathcal{H}_Q$ in the I_z basis can be arranged in a block diagonal form for $I = p/2$, p odd [7,9]. The calculations reported in this paper were performed with the use of linear algebra functions provided within the *Mathematica* programming environment [14].

Numerical diagonalization functions return the $(2I + 1)$ computed eigenvectors of a matrix in an order that may be unpredictable. A procedure must therefore be devised to definitively relate a given eigenvector $|\psi_n(\eta)\rangle$ to its "parent" state $|n\rangle$. Since the eigenvectors are by definition orthonormal, the projection of the kth basis vector onto $|\psi_n(\eta_0)\rangle$, $\eta_0 \sim 0$, should be close to unity only if $n = k$ and zero otherwise, that is

$$|\langle k|\psi_n(\eta_0)\rangle| \approx \delta_{kn}, \tag{5}$$

where δ_{kn} is the Dirac delta function. This procedure may be iterated, beginning with $\eta = 0$ and evaluating the inner products while incrementing the asymmetry parameter in steps of η_0. The criterion for deciding the parent state in the $(p+1)$th iterate in this procedure would be:

$$|\langle \psi_k(p\eta_0)|\psi_n((p+1)\eta_0)\rangle| \approx \delta_{kn}, \tag{6}$$

with p being incremented from 0 to $(\eta_0^{-1} - 1)$. In this way, the eigenstates and eigenvalues of $\mathcal{H}_Q$ can be unambiguously assigned to their parent state for each $p\eta_0$ increment from 0 to 1, even for the pairs of states $|\psi_{\pm n}(\eta)\rangle$, which are degenerate for spins with half integral I. The *Mathematica* codes developed for this work incorporate this procedure to perform the sorting and assignment tasks in an automated fashion.
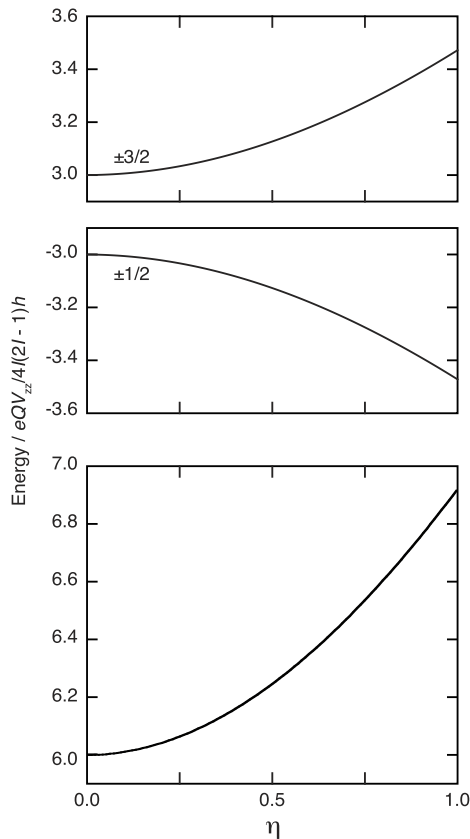
Fig. 1. Eigenvalues and single-quantum transition energies of $\mathcal{H}_Q$ for $I = 3/2$ as a function of η. Functions plotted are: $\lambda_{\pm 3/2}(\eta)$ (*top*); $\lambda_{\pm 1/2}(\eta)$ (*middle*); and $\lambda_{\pm 3/2}(\eta) - \lambda_{\pm 1/2}(\eta)$ (*bottom*).

3. Results and discussion

3.1. Spin-3/2

Exact solutions for the doubly degenerate eigenvalues of $\mathcal{H}_Q$ have been derived for $I = 3/2$ [9]; in frequency units, they are

$$\lambda_{\pm 3/2}(\eta) = \frac{eQV_{zz}}{4h}\left(1 + \frac{\eta^2}{3}\right)^{1/2}, \tag{7}$$

$$\lambda_{\pm 1/2}(\eta) = -\frac{eQV_{zz}}{4h}\left(1 + \frac{\eta^2}{3}\right)^{1/2}. \tag{8}$$

These functions and the allowed (single-quantum) transition energies are plotted as functions of η in Fig. 1, and a list of $(\eta, \lambda_{\pm m}(\eta))$ pairs is presented in Table 1. Magnitudes of the coefficients $c_{nk}(\eta)$ (Eq. (4)) are displayed in Fig. 2. Measurement of the single allowed transition for $I = 3/2$ does not suffice to determine the two variables V_{zz} and η, although η can often be independently evaluated by *ab initio* calculations or through consideration of the symmetry of the nuclide's environment [15].

3.2. Spin-5/2

The numerical evaluation of the energy levels and allowed transition energies of $\mathcal{H}_Q$ for $I = 5/2$ are summarized by Table 2 and the plots in Fig. 3. The dependence of $|\langle k|\psi_n(\eta)\rangle|$ on η is illustrated in Fig. 4. Unlike the case for $I = 3/2$, a spin-5/2 nuclide should exhibit two allowed NQR transitions, except for cases where $\eta = 1$, when the two transitions have the same energy. Thus, V_{zz} and η can be uniquely and reliably determined from the NQR spectrum.
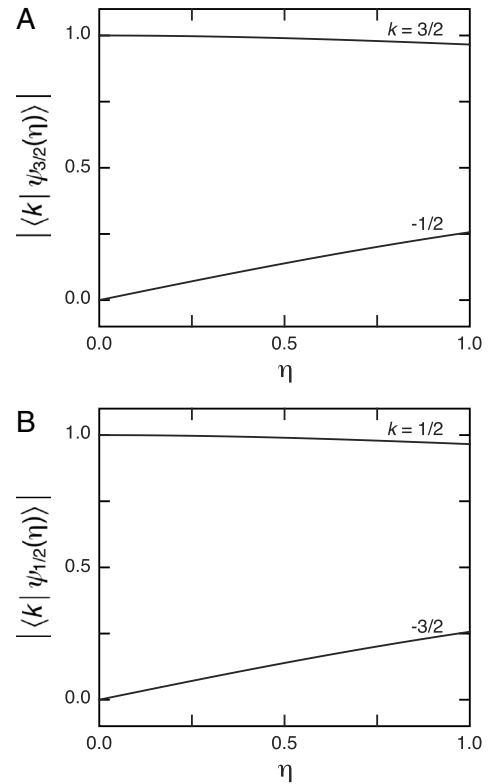
Fig. 2. Magnitudes of the complex coefficients $c_{nk}(\eta)$ of Eq. (2) for $I = 3/2$. Results are shown for the $|\psi_{3/2}(\eta)\rangle$ (A) and $|\psi_{1/2}(\eta)\rangle$ (B) eigenstates of $\mathcal{H}_Q$.

3.3. Spin-7/2

Nuclides with $I = 7/2$ have eight doubly degenerate eigenstates and exhibit three distinct allowed transitions (Fig. 5 and Table 3). The energy curve of the $\pm 3/2 \leftrightarrow \pm 1/2$ transition intersects the $\pm 5/2 \leftrightarrow \pm 3/2$ and the $\pm 7/2 \leftrightarrow \pm 5/2$ curves at $\eta \approx 0.585$ and $\eta = 1$, respectively.

Fig. 6 reveals that the expansions of the energy eigenstates $|\psi_n(\eta)\rangle$ can include significant contributions from states other than $|n\rangle$. The degree of mixing of the $n = \pm I$ states with the other I_z basis states is small, but can be over 50% for other values of n. In all cases the only coefficients $c_{nk}(\eta)$ found to be non-zero were those for which $k = n \pm 2q$, as predicted in Section 2.

The finite size of the $|c_{nk}(\eta)|$, $k \neq n$, suggests that certain dipole forbidden NQR transitions can become weakly allowed when $\eta \neq 0$ [13]. Whereas allowed NQR transitions are characterized by changes in the spin angular quantum number of $\triangle m = \pm 1$, the mixing of states separated by angular momenta quanta of $2q$ leads to non-zero magnetic dipole matrix elements between pairs of states with $\triangle m = \pm q$, q odd. For some pairs of states, such as $\left(|\psi_{3/2}(\eta)\rangle, |\psi_{-3/2}(\eta)\rangle\right)$ the energy of the forbidden transition may be small or zero, but for others, e.g., $\left(|\psi_{7/2}(\eta)\rangle, |\psi_{1/2}(\eta)\rangle\right)$, the energy difference may be much larger than any of the allowed transitions. The intensities of the resonances would serve to differentiate allowed from forbidden transitions.

3.4. Spin-9/2

The five doubly degenerate energy levels and four allowed zero field transition energies of a spin-9/2 nuclide are plotted in Fig. 7 as functions of η. A numerical list of the energy eigenvalues is given in Table 4. The bottom figure shows that the energy difference $\lambda_{\pm 3/2}(\eta) - \lambda_{\pm 1/2}(\eta)$ is the lowest of the four transitions for small η, but transects the curves of the other transitions and joins the
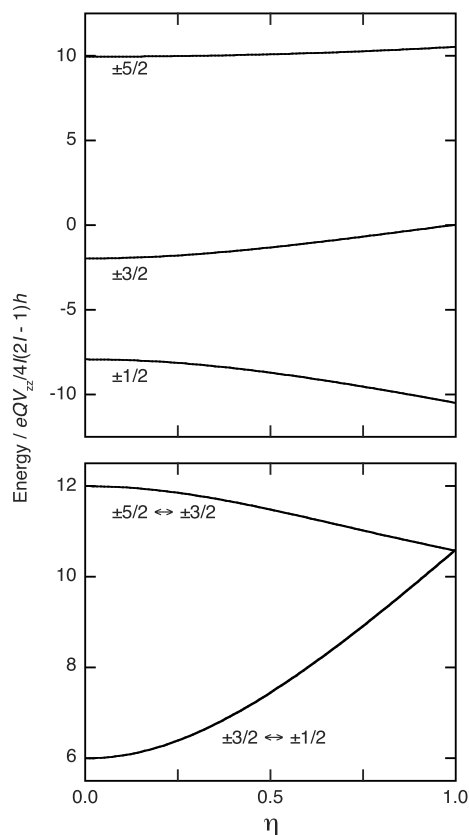
Fig. 3. Eigenvalues (*top*) and single-quantum transition energies (*bottom*) of $\mathcal{H}_Q$ for spin-5/2 as a function of η. Plots of the eigenvalue functions $\lambda_m(\eta)$ are labeled according to their m values and plots of the transition energies are labeled by the connected states $|\psi_m(\eta)\rangle$ and $|\psi_{m-1}(\eta)\rangle$.

highest lying $\lambda_{\pm 9/2}(\eta) - \lambda_{\pm 7/2}(\eta)$ difference function at $\eta = 1$. Similar behavior is observed in the previous plots of transition energies, where the energy curve for the $|\psi_{\pm 1/2}(\eta)\rangle \leftrightarrow |\psi_{\pm 3/2}(\eta)\rangle$ transition is always lowest at $\eta = 0$ but becomes larger and crosses the other curves as η increases until it becomes degenerate with the $|\psi_{\pm(I-1)}(\eta)\rangle \leftrightarrow |\psi_{\pm I}(\eta)\rangle$ transition at $\eta = 1$.

The crossing of energy curves is made possible by the much larger variability in $\lambda_{\pm 3/2}(\eta) - \lambda_{\pm 1/2}(\eta)$ as compared to the energies of other transitions. Because of the potential for the energy curves to cross, in any analysis of NQR spectra there will be inherent uncertainty in identifying which eigenstate pairs to assign to a given resonance. As a result, detection of only two NQR signals may not suffice to determine the two parameters η and V_{zz}; observation of a third transition or the introduction of additional information that would enable η to be estimated would be needed for an unambiguous extraction of EFG parameters.

As seen for the $I = 7/2$ case, expansion of the energy eigenstates reveals substantial mixing of the $|m\rangle$ basis states (Fig. 8), indicating that dipole forbidden odd order transitions can have a finite probability for non-zero η.

4. Conclusion

Tables 1–4 provide data required to interpret NQR spectra and determine EFG tensors from the experimentally measured transition frequencies. Complications in the analysis can arise when spectra are incomplete or ambiguous: lines may be missing because of unfavorable relaxation times or frequencies that lie outside the bandwidth of the spectrometer; the order of resonances

Fig. 4. Magnitudes of the complex coefficients $c_{nk}(\eta)$ of Eq. (2) for $I = 5/2$. Results are shown for the $|\psi_{5/2}(\eta)\rangle$ (A), $|\psi_{3/2}(\eta)\rangle$ (B), and $|\psi_{1/2}(\eta)\rangle$ (C) eigenstates of $\mathcal{H}_Q$.

Table A

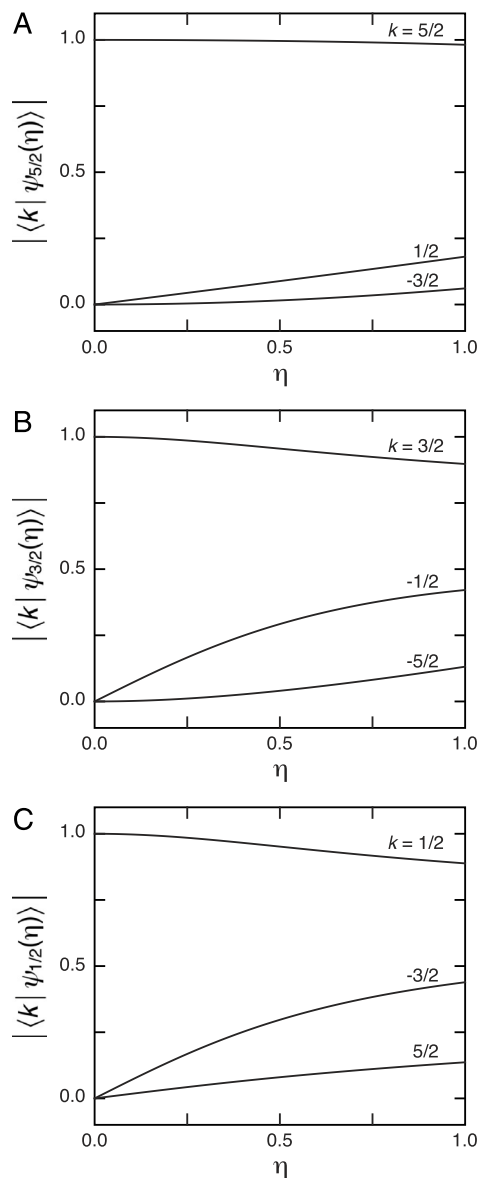Data for long-lived radioisotopes relevant to NQR and NMR spectroscopy [4,5].

Isotope	Spin of nuclear ground state	Quadrupole moment ($\times 10^{-28}$ m^2)	Gyromagnetic ratio ($\times 10^3$ rad s^{-1} mT^{-1})
^{99}Tc	$\frac{9}{2}$	0.129	60.504
^{227}Ac	$\frac{3}{2}$	1.700	35.123
^{229}Th	$\frac{5}{2}$	4.300	8.813
^{231}Pa	$\frac{3}{2}$	−1.720	64.179
^{233}U	$\frac{5}{2}$	3.663	11.303
^{235}U	$\frac{7}{2}$	4.936	4.653–6.295
^{237}Np	$\frac{5}{2}$	3.886	60.156

might be scrambled due to crossing of transition energies; extra lines may be present from forbidden transitions. In such cases, the energy functions and eigenstate expansions shown in Figs. 1–8 can be essential in resolving uncertainties and assigning lines to the correct transitions.

Nuclides with large quadrupole moments and high field gradients are the most favorable for NQR spectroscopy, as exempli-
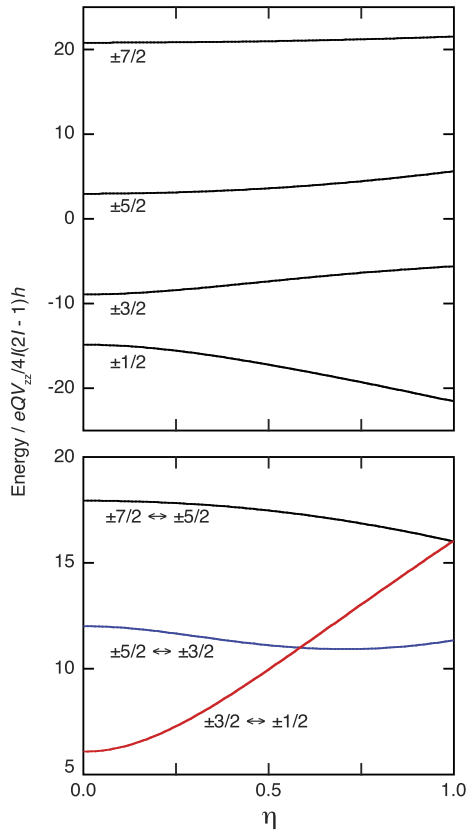
Fig. 5. Eigenvalues (*top*) and single-quantum transition energies (*bottom*) of $\mathcal{H}_Q$ for spin-7/2 as a function of η. Plots of the eigenvalue functions $\lambda_m(\eta)$ are labeled according to their m values and plots of the transition energies are labeled by the connected states $|\psi_m(\eta)\rangle$ and $|\psi_{m-1}(\eta)\rangle$.
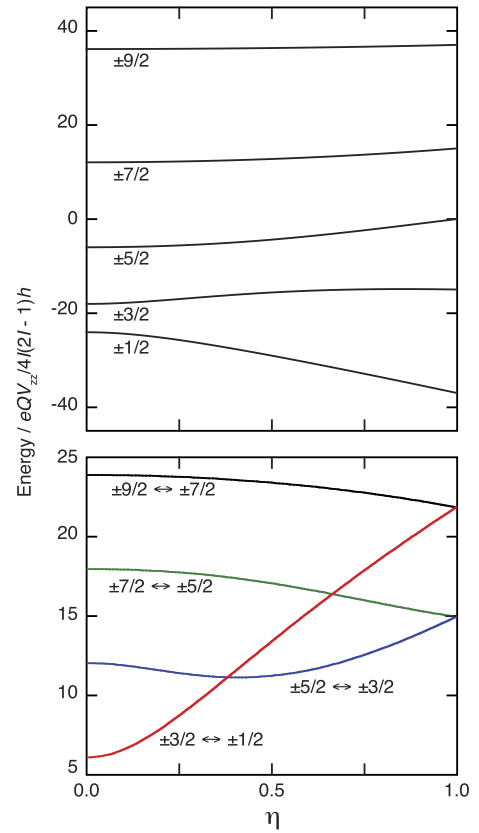
Fig. 7. Eigenvalues (*top*) and single-quantum transition energies (*bottom*) of $\mathcal{H}_Q$ for spin-9/2 as a function of η. Plots of the eigenvalue functions $\lambda_m(\eta)$ are labeled according to their m values and plots of the transition energies are labeled by the connected states $|\psi_m(\eta)\rangle$ and $|\psi_{m-1}(\eta)\rangle$.
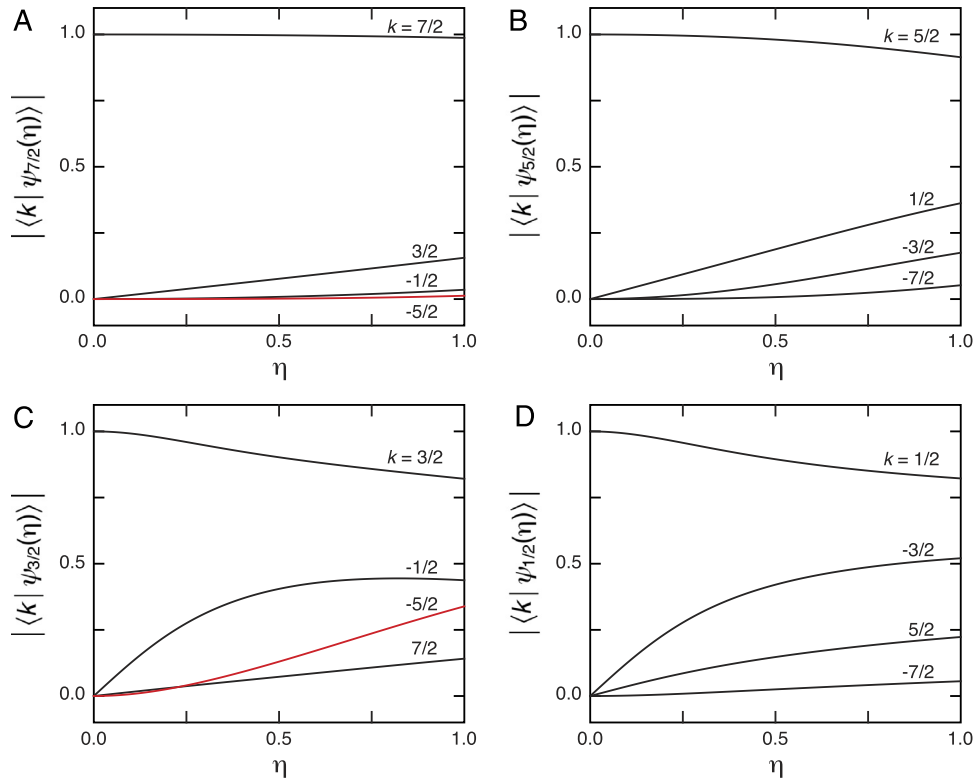
Fig. 6. Magnitudes of the complex coefficients $c_{nk}(\eta)$ of Eq. (2) for $I = 7/2$. Results are shown for the $|\psi_{7/2}(\eta)\rangle$ (A), $|\psi_{5/2}(\eta)\rangle$ (B), $|\psi_{3/2}(\eta)\rangle$ (C), and $|\psi_{1/2}(\eta)\rangle$ (D) eigenstates of $\mathcal{H}_Q$.
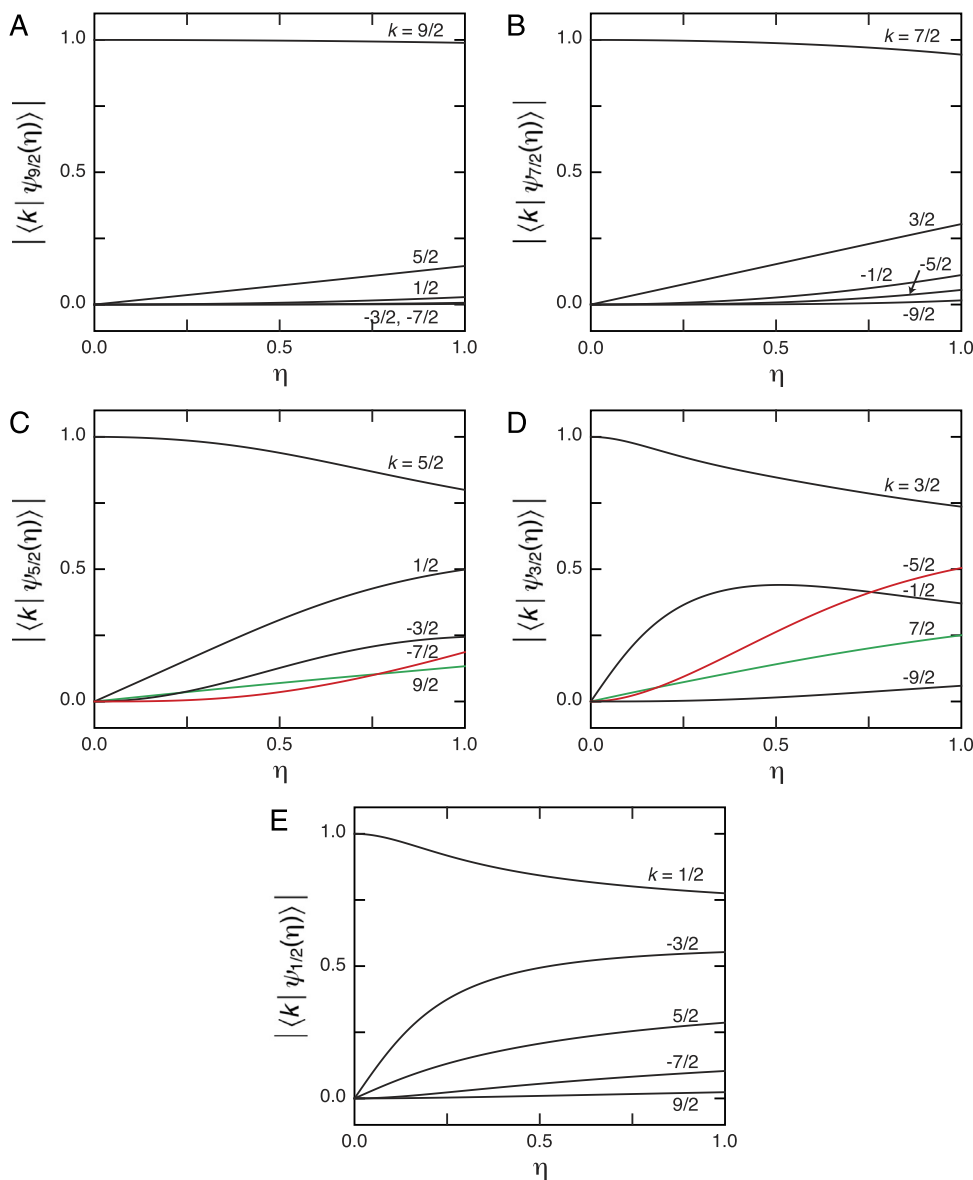
Fig. 8. Magnitudes of the complex coefficients $c_{nk}(\eta)$ of Eq. (2) for $I = 9/2$. Results are shown for the $|\psi_{9/2}(\eta)\rangle$ (A) $|\psi_{7/2}(\eta)\rangle$ (B), $|\psi_{5/2}(\eta)\rangle$ (C), $|\psi_{3/2}(\eta)\rangle$ (D), and $|\psi_{1/2}(\eta)\rangle$ (E) eigenstates of $\mathcal{H}_Q$.

fied by the longstanding attention on the halogen isotopes ^{35,37}Cl, ^{79,81}Br, and ^{127}I [1,2]. Although previous NQR studies have focused exclusively on stable light isotopes, several heavy radionuclides have exceptionally large quadrupole moments suggesting that they too would be promising candidates for NQR experiments. Most of these isotopes, shown in Table A, are available in quantities sufficient for detection by NQR instruments. The magnitude of the NQR transition energies expected for these nuclides can be estimated with EFG tensors computed by *ab initio* methods. Assuming the relativistic results obtained by de Jong et al. [16] and Autschbach et al. [17] for uranium in the uranyl (UO_2^{2+}) ion, ^{233}U and ^{235}U zero field splittings on the order of 10^2–10^3 MHz are predicted (Table B). Quadrupole couplings of this size would be significantly greater than the energy due to the Zeeman interaction, which in a 11.74 T NMR magnet, would be 21.12 and 8.70–11.76 MHz for ^{233}U and ^{235}U, respectively. These results suggest that pure NQR experiments would be a more attractive option than NMR spectroscopy for probing the complex electronic structure of the 5f elements [18–22]. Methods demonstrating the feasibility of ra-

diofrequency spectroscopic experiments such as NMR and NQR on highly radioactive samples have been described [23–26].

As EFG tensor calculations improve, it becomes feasible to consider NQR experiments as a way to accurately measure nuclear quadrupole moments [2,3]. Current reference values of nuclear data for quadrupolar actinide isotopes (and radioisotopes generally) are characterized by large uncertainties or wide variation from method to method [4,5]. Nuclear transition energies, which typically appear in the radiofrequency part of the electromagnetic spectrum, are usually well-resolved, and should provide a straightforward way for determining Q, limited in accuracy only by the quality of the calculation of the parameter V_{zz} [17,15,27].

Acknowledgments

Table B
Calculated magnetic dipole allowed NQR transition frequencies (in MHz) for uranium isotopes in axially symmetric U(VI) environments.

Uranyl ion	^{233}U		^{235}U		
	$\pm\frac{1}{2} \leftrightarrow \pm\frac{3}{2}$	$\pm\frac{3}{2} \leftrightarrow \pm\frac{5}{2}$	$\pm\frac{1}{2} \leftrightarrow \pm\frac{3}{2}$	$\pm\frac{3}{2} \leftrightarrow \pm\frac{5}{2}$	$\pm\frac{5}{2} \leftrightarrow \pm\frac{7}{2}$
UO_2^{2+} [16]	351.1	702.2	225.3	450.6	676.0
$(UO_2(HCO_3)_3)^-$ [17]	1075.6	2151.3	690.2	1380.4	2070.6

References

[1] R. Pound, Phys. Rev. 79 (4) (1950) 685.
[2] T.P. Das, E.L. Hahn, Nuclear Quadrupole Resonance Spectroscopy, no. I, Academic Press, Elsevier, New York, 1958.
[3] C.H. Townes, Determination of Nuclear Quadrupole Moments, in: External Properties of Atomic Nuclei/Äussere Eigenschaften der Atomkerne, Springer, 1958, pp. 377–453.
[4] P. Raghavan, At. Data Nucl. Data Tables 42 (2) (1989) 189–291.
[5] P. Pyykkö, Mol. Phys. 106 (16–18) (2008) 1965–1974.
[6] M. Cohen, F. Reif, Solid State Phys. 5 (1957) 321–438.
[7] R. Bersohn, J. Chem. Phys. 20 (10) (1952) 1505–1509.
[8] M. Cohen, Phys. Rev. 96 (5) (1954) 1278.
[9] T.-C. Wang, Phys. Rev. 99 (2) (1955) 566.
[10] R. Livingston, H. Zeldes, Table of Eigenvalues for Pure Quadrupole Spectra, Spin 5/2, Oak Ridge National Laboratory, Oak Ridge, 1955.
[11] G. Shenoy, B. Dunlap, Nucl. Instrum. Methods 71 (3) (1969) 285–291.
[12] E. Harel, H. Cho, J. Magn. Reson. 183 (2) (2006) 308–314.
[13] F.A. Perras, C.M. Widdifield, D.L. Bryce, Solid State Nucl. Magn. Reson. 45 (2012) 36–44.
[14] Wolfram Research, Inc., Mathematica, Version 8.0, Wolfram Research, Inc., Champaign, Illinois, 2010.
[15] J. Autschbach, S. Zheng, R.W. Schurko, Concepts Magn. Res. A 36 (2) (2010) 84–126.
[16] W. de Jong, L. Visscher, W. Nieuwpoort, J. Mol. Struct. THEOCHEM 458 (1) (1999) 41–52.
[17] J. Autschbach, P. Daoling, M. Reiher, J. Chem. Theory Comput. 8 (11) (2012) 4239–4248.
[18] A.J. Freeman, J.B. Darby Jr. (Eds.), The Actinides: Electronic Structure and Related Properties, Vol. 2, Academic Press, New York, 1974.
[19] M. Pepper, B.E. Bursten, Chem. Rev. 91 (5) (1991) 719–741.
[20] V.G. Pershina, Chem. Rev. 96 (6) (1996) 1977–2010.
[21] N. Kaltsoyannis, Chem. Soc. Rev. 32 (1) (2003) 9–16.
[22] M. Dolg (Ed.), Computational Methods in Lanthanide and Actinide Chemistry, John Wiley & Sons Ltd., Chichester, West Sussex, 2015.
[23] I. Farnan, H. Cho, W.J. Weber, R.D. Scheele, N.R. Johnson, A.E. Kozelisky, Rev. Sci. Instrum. 75 (12) (2004) 5232–5236. http://dx.doi.org/10.1063/1.1818512.
[24] H. Cho, W.A. de Jong, C.Z. Soderquist, J. Chem. Phys. 132 (2010) 084501.
[25] H. Cho, W.A. de Jong, A.P. Sattelberger, F. Poineau, K.R. Czerwinski, J. Am. Chem. Soc. 132 (38) (2010) 13138–13140. http://dx.doi.org/10.1021/ja105687j.
[26] L. Martel, J. Somers, C. Berkmann, F. Koepp, A. Rothermel, O. Pauvert, C. Selfslag, I. Farnan, Rev. Sci. Instrum. 84 (2013) 055112. http://dx.doi.org/10.1063/1.4805017.
[27] F. Aquino, N. Govind, J. Autschbach, J. Chem. Theory Comput. 6 (9) (2010) 2669–2686.

Explanation of Tables

Table 1.   **List of the energy eigenvalues of the quadrupolar Hamiltonian for $m = 3/2$ as a function of η, as plotted in** Fig. 1**.**

         η EFG tensor asymmetry parameter
         $\pm 1/2$ Eigenvalues of $|\psi_{\pm 1/2}(\eta)\rangle$ states in units of $eQV_{zz}/4I(2I-1)h$
         $\pm 3/2$ Eigenvalues of $|\psi_{\pm 3/2}(\eta)\rangle$ states in units of $eQV_{zz}/4I(2I-1)h$

Table 2.   **List of the energy eigenvalues of the quadrupolar Hamiltonian for $m = 5/2$ as a function of η, as plotted in** Fig. 3**.**

         η EFG tensor asymmetry parameter
         $\pm 5/2$ Eigenvalues of $|\psi_{\pm 5/2}(\eta)\rangle$ states in units of $eQV_{zz}/4I(2I-1)h$
         $\pm 1/2$ Eigenvalues of $|\psi_{\pm 1/2}(\eta)\rangle$ states in units of $eQV_{zz}/4I(2I-1)h$
         $\pm 3/2$ Eigenvalues of $|\psi_{\pm 3/2}(\eta)\rangle$ states in units of $eQV_{zz}/4I(2I-1)h$

Table 3.   **List of the energy eigenvalues of the quadrupolar Hamiltonian for $m = 7/2$ as a function of η, as plotted in** Fig. 5**.**

         η EFG tensor asymmetry parameter
         $\pm 7/2$ Eigenvalues of $|\psi_{\pm 7/2}(\eta)\rangle$ states in units of $eQV_{zz}/4I(2I-1)h$
         $\pm 1/2$ Eigenvalues of $|\psi_{\pm 1/2}(\eta)\rangle$ states in units of $eQV_{zz}/4I(2I-1)h$
         $\pm 3/2$ Eigenvalues of $|\psi_{\pm 3/2}(\eta)\rangle$ states in units of $eQV_{zz}/4I(2I-1)h$
         $\pm 5/2$ Eigenvalues of $|\psi_{\pm 5/2}(\eta)\rangle$ states in units of $eQV_{zz}/4I(2I-1)h$

Table 4.   **List of the energy eigenvalues of the quadrupolar Hamiltonian for $m = 9/2$ as a function of η, as plotted in** Fig. 7**.**

         η EFG tensor asymmetry parameter
         $\pm 9/2$ Eigenvalues of $|\psi_{\pm 9/2}(\eta)\rangle$ states in units of $eQV_{zz}/4I(2I-1)h$
         $\pm 1/2$ Eigenvalues of $|\psi_{\pm 1/2}(\eta)\rangle$ states in units of $eQV_{zz}/4I(2I-1)h$
         $\pm 3/2$ Eigenvalues of $|\psi_{\pm 3/2}(\eta)\rangle$ states in units of $eQV_{zz}/4I(2I-1)h$
         $\pm 7/2$ Eigenvalues of $|\psi_{\pm 7/2}(\eta)\rangle$ states in units of $eQV_{zz}/4I(2I-1)h$
         $\pm 5/2$ Eigenvalues of $|\psi_{\pm 5/2}(\eta)\rangle$ states in units of $eQV_{zz}/4I(2I-1)h$

Table 1
List of the energy eigenvalues of the quadrupolar Hamiltonian for $m = 3/2$ as a function of η, as plotted in Fig. 1.

η	$\pm 1/2$	$\pm 3/2$		η	$\pm 1/2$	$\pm 3/2$
0.000	−3.000	3.000		0.510	−3.130	3.130
0.010	−3.000	3.000		0.520	−3.135	3.135
0.020	−3.000	3.000		0.530	−3.140	3.140
0.030	−3.001	3.001		0.540	−3.145	3.145
0.040	−3.001	3.001		0.550	−3.150	3.150
0.050	−3.002	3.002		0.560	−3.155	3.155
0.060	−3.002	3.002		0.570	−3.161	3.161
0.070	−3.003	3.003		0.580	−3.166	3.166
0.080	−3.004	3.004		0.590	−3.172	3.172
0.090	−3.005	3.005		0.600	−3.177	3.177
0.100	−3.006	3.006		0.610	−3.183	3.183
0.110	−3.007	3.007		0.620	−3.189	3.189
0.120	−3.008	3.008		0.630	−3.194	3.194
0.130	−3.010	3.010		0.640	−3.200	3.200
0.140	−3.011	3.011		0.650	−3.206	3.206
0.150	−3.013	3.013		0.660	−3.213	3.213
0.160	−3.014	3.014		0.670	−3.219	3.219
0.170	−3.016	3.016		0.680	−3.225	3.225
0.180	−3.018	3.018		0.690	−3.231	3.231
0.190	−3.020	3.020		0.700	−3.238	3.238
0.200	−3.022	3.022		0.710	−3.244	3.244
0.210	−3.024	3.024		0.720	−3.251	3.251
0.220	−3.026	3.026		0.730	−3.257	3.257
0.230	−3.028	3.028		0.740	−3.264	3.264
0.240	−3.030	3.030		0.750	−3.271	3.271
0.250	−3.033	3.033		0.760	−3.278	3.278
0.260	−3.036	3.036		0.770	−3.285	3.285
0.270	−3.038	3.038		0.780	−3.292	3.292
0.280	−3.041	3.041		0.790	−3.299	3.299
0.290	−3.044	3.044		0.800	−3.306	3.306
0.300	−3.047	3.047		0.810	−3.313	3.313
0.310	−3.050	3.050		0.820	−3.321	3.321
0.320	−3.053	3.053		0.830	−3.328	3.328
0.330	−3.056	3.056		0.840	−3.335	3.335
0.340	−3.059	3.059		0.850	−3.343	3.343
0.350	−3.063	3.063		0.860	−3.351	3.351
0.360	−3.066	3.066		0.870	−3.358	3.358
0.370	−3.070	3.070		0.880	−3.366	3.366
0.380	−3.074	3.074		0.890	−3.374	3.374
0.390	−3.077	3.077		0.900	−3.382	3.382
0.400	−3.081	3.081		0.910	−3.390	3.390
0.410	−3.085	3.085		0.920	−3.398	3.398
0.420	−3.089	3.089		0.930	−3.406	3.406
0.430	−3.093	3.093		0.940	−3.414	3.414
0.440	−3.098	3.098		0.950	−3.422	3.422
0.450	−3.102	3.102		0.960	−3.430	3.430
0.460	−3.106	3.106		0.970	−3.439	3.439
0.470	−3.111	3.111		0.980	−3.447	3.447
0.480	−3.115	3.115		0.990	−3.456	3.456
0.490	−3.120	3.120		1.000	−3.464	3.464
0.500	−3.125	3.125				

Table 2
List of the energy eigenvalues of the quadrupolar Hamiltonian for $m = 5/2$ as a function of η, as plotted in Fig. 3.

η	$\pm 5/2$	$\pm 1/2$	$\pm 3/2$	η	$\pm 5/2$	$\pm 1/2$	$\pm 3/2$
0.000	10.000	−8.000	−2.000	0.510	10.146	−8.824	−1.322
0.010	10.000	−8.000	−2.000	0.520	10.152	−8.854	−1.299
0.020	10.000	−8.001	−1.999	0.530	10.158	−8.883	−1.275
0.030	10.001	−8.003	−1.997	0.540	10.164	−8.913	−1.251
0.040	10.001	−8.006	−1.995	0.550	10.171	−8.944	−1.227
0.050	10.001	−8.009	−1.993	0.560	10.177	−8.975	−1.202
0.060	10.002	−8.013	−1.989	0.570	10.184	−9.006	−1.178
0.070	10.003	−8.017	−1.985	0.580	10.190	−9.037	−1.153
0.080	10.004	−8.023	−1.981	0.590	10.197	−9.069	−1.128
0.090	10.005	−8.029	−1.976	0.600	10.204	−9.101	−1.103
0.100	10.006	−8.035	−1.970	0.610	10.211	−9.133	−1.077
0.110	10.007	−8.043	−1.964	0.620	10.218	−9.166	−1.052
0.120	10.008	−8.051	−1.957	0.630	10.225	−9.199	−1.026
0.130	10.009	−8.060	−1.950	0.640	10.232	−9.232	−1.000
0.140	10.011	−8.069	−1.942	0.650	10.240	−9.266	−0.974
0.150	10.013	−8.079	−1.933	0.660	10.247	−9.300	−0.948
0.160	10.014	−8.090	−1.924	0.670	10.255	−9.334	−0.921
0.170	10.016	−8.101	−1.915	0.680	10.263	−9.368	−0.895
0.180	10.018	−8.113	−1.905	0.690	10.271	−9.403	−0.868
0.190	10.020	−8.126	−1.894	0.700	10.279	−9.438	−0.841
0.200	10.022	−8.139	−1.883	0.710	10.287	−9.473	−0.814
0.210	10.025	−8.153	−1.871	0.720	10.296	−9.508	−0.787
0.220	10.027	−8.168	−1.859	0.730	10.304	−9.544	−0.760
0.230	10.029	−8.183	−1.846	0.740	10.313	−9.580	−0.733
0.240	10.032	−8.199	−1.833	0.750	10.321	−9.616	−0.705
0.250	10.035	−8.215	−1.820	0.760	10.330	−9.653	−0.678
0.260	10.038	−8.232	−1.805	0.770	10.339	−9.689	−0.650
0.270	10.041	−8.250	−1.791	0.780	10.348	−9.726	−0.623
0.280	10.044	−8.268	−1.776	0.790	10.358	−9.763	−0.595
0.290	10.047	−8.287	−1.760	0.800	10.367	−9.800	−0.567
0.300	10.050	−8.306	−1.744	0.810	10.377	−9.838	−0.539
0.310	10.054	−8.326	−1.728	0.820	10.386	−9.875	−0.511
0.320	10.057	−8.346	−1.711	0.830	10.396	−9.913	−0.483
0.330	10.061	−8.367	−1.694	0.840	10.406	−9.951	−0.455
0.340	10.065	−8.389	−1.676	0.850	10.416	−9.989	−0.427
0.350	10.068	−8.411	−1.658	0.860	10.426	−10.028	−0.399
0.360	10.072	−8.433	−1.640	0.870	10.436	−10.066	−0.370
0.370	10.077	−8.456	−1.621	0.880	10.447	−10.105	−0.342
0.380	10.081	−8.479	−1.602	0.890	10.458	−10.144	−0.314
0.390	10.085	−8.503	−1.582	0.900	10.468	−10.183	−0.285
0.400	10.090	−8.528	−1.562	0.910	10.479	−10.222	−0.257
0.410	10.094	−8.552	−1.542	0.920	10.490	−10.262	−0.228
0.420	10.099	−8.578	−1.521	0.930	10.501	−10.301	−0.200
0.430	10.104	−8.603	−1.500	0.940	10.512	−10.341	−0.171
0.440	10.109	−8.630	−1.479	0.950	10.524	−10.381	−0.143
0.450	10.114	−8.656	−1.458	0.960	10.535	−10.421	−0.114
0.460	10.119	−8.683	−1.436	0.970	10.547	−10.461	−0.086
0.470	10.124	−8.711	−1.414	0.980	10.559	−10.502	−0.057
0.480	10.130	−8.738	−1.391	0.990	10.571	−10.542	−0.029
0.490	10.135	−8.767	−1.368	1.000	10.583	−10.583	0.000
0.500	10.141	−8.795	−1.345				

Table 3
List of the energy eigenvalues of the quadrupolar Hamiltonian for $m = 7/2$ as a function of η, as plotted in Fig. 5.

η	$\pm7/2$	$\pm1/2$	$\pm3/2$	$\pm5/2$	η	$\pm7/2$	$\pm1/2$	$\pm3/2$	$\pm5/2$
0.000	21.000	−15.000	−9.000	3.000	0.510	21.184	−17.451	−7.403	3.670
0.010	21.000	−15.001	−8.999	3.000	0.520	21.191	−17.529	−7.360	3.697
0.020	21.000	−15.005	−8.996	3.001	0.530	21.198	−17.607	−7.316	3.725
0.030	21.001	−15.011	−8.992	3.002	0.540	21.206	−17.686	−7.273	3.753
0.040	21.001	−15.020	−8.985	3.004	0.550	21.214	−17.766	−7.231	3.782
0.050	21.002	−15.031	−8.977	3.006	0.560	21.222	−17.846	−7.188	3.812
0.060	21.003	−15.045	−8.967	3.009	0.570	21.230	−17.926	−7.145	3.842
0.070	21.003	−15.061	−8.955	3.012	0.580	21.238	−18.007	−7.103	3.872
0.080	21.004	−15.079	−8.941	3.016	0.590	21.246	−18.089	−7.061	3.904
0.090	21.006	−15.100	−8.926	3.020	0.600	21.255	−18.171	−7.019	3.935
0.100	21.007	−15.123	−8.909	3.025	0.610	21.264	−18.254	−6.978	3.968
0.110	21.008	−15.148	−8.891	3.030	0.620	21.273	−18.337	−6.937	4.001
0.120	21.010	−15.176	−8.870	3.036	0.630	21.282	−18.420	−6.896	4.034
0.130	21.012	−15.205	−8.849	3.042	0.640	21.291	−18.504	−6.855	4.068
0.140	21.014	−15.237	−8.826	3.049	0.650	21.300	−18.588	−6.815	4.103
0.150	21.016	−15.271	−8.801	3.056	0.660	21.309	−18.673	−6.775	4.138
0.160	21.018	−15.307	−8.775	3.064	0.670	21.319	−18.758	−6.735	4.174
0.170	21.020	−15.345	−8.748	3.073	0.680	21.329	−18.843	−6.696	4.210
0.180	21.023	−15.385	−8.719	3.081	0.690	21.339	−18.929	−6.657	4.247
0.190	21.025	−15.426	−8.690	3.091	0.700	21.349	−19.015	−6.618	4.284
0.200	21.028	−15.470	−8.659	3.101	0.710	21.359	−19.101	−6.580	4.322
0.210	21.031	−15.515	−8.627	3.111	0.720	21.369	−19.188	−6.542	4.361
0.220	21.034	−15.562	−8.594	3.122	0.730	21.380	−19.275	−6.505	4.400
0.230	21.037	−15.610	−8.560	3.133	0.740	21.390	−19.362	−6.468	4.440
0.240	21.040	−15.660	−8.525	3.145	0.750	21.401	−19.450	−6.431	4.480
0.250	21.044	−15.712	−8.489	3.158	0.760	21.412	−19.538	−6.395	4.521
0.260	21.047	−15.765	−8.453	3.171	0.770	21.423	−19.626	−6.359	4.562
0.270	21.051	−15.820	−8.416	3.184	0.780	21.435	−19.715	−6.324	4.604
0.280	21.055	−15.876	−8.378	3.198	0.790	21.446	−19.804	−6.289	4.647
0.290	21.059	−15.933	−8.339	3.213	0.800	21.458	−19.893	−6.255	4.690
0.300	21.063	−15.991	−8.300	3.228	0.810	21.470	−19.982	−6.221	4.733
0.310	21.067	−16.051	−8.260	3.243	0.820	21.482	−20.072	−6.187	4.777
0.320	21.072	−16.112	−8.219	3.259	0.830	21.494	−20.162	−6.154	4.822
0.330	21.077	−16.174	−8.178	3.276	0.840	21.506	−20.252	−6.121	4.867
0.340	21.081	−16.237	−8.137	3.293	0.850	21.518	−20.343	−6.089	4.913
0.350	21.086	−16.302	−8.095	3.311	0.860	21.531	−20.433	−6.057	4.959
0.360	21.091	−16.367	−8.053	3.329	0.870	21.544	−20.524	−6.026	5.006
0.370	21.096	−16.434	−8.011	3.348	0.880	21.557	−20.615	−5.995	5.053
0.380	21.102	−16.501	−7.968	3.368	0.890	21.570	−20.707	−5.964	5.101
0.390	21.107	−16.569	−7.925	3.388	0.900	21.583	−20.798	−5.934	5.150
0.400	21.113	−16.638	−7.882	3.408	0.910	21.596	−20.890	−5.905	5.198
0.410	21.118	−16.708	−7.839	3.429	0.920	21.610	−20.982	−5.876	5.248
0.420	21.124	−16.779	−7.796	3.451	0.930	21.624	−21.074	−5.847	5.298
0.430	21.130	−16.851	−7.752	3.473	0.940	21.638	−21.166	−5.819	5.348
0.440	21.136	−16.923	−7.708	3.495	0.950	21.652	−21.259	−5.791	5.399
0.450	21.143	−16.997	−7.665	3.519	0.960	21.666	−21.352	−5.764	5.450
0.460	21.149	−17.071	−7.621	3.543	0.970	21.680	−21.445	−5.738	5.502
0.470	21.156	−17.145	−7.577	3.567	0.980	21.695	−21.538	−5.711	5.554
0.480	21.163	−17.221	−7.534	3.592	0.990	21.710	−21.631	−5.685	5.607
0.490	21.169	−17.297	−7.490	3.617	1.000	21.725	−21.725	−5.660	5.660
0.500	21.176	−17.373	−7.447	3.643					

Table 4
List of the energy eigenvalues of the quadrupolar Hamiltonian for $m = 9/2$ as a function of η, as plotted in Fig. 7.

η	$\pm9/2$	$\pm1/2$	$\pm3/2$	$\pm7/2$	$\pm5/2$	η	$\pm9/2$	$\pm1/2$	$\pm3/2$	$\pm7/2$	$\pm5/2$
0.000	36.000	−24.000	−18.000	12.000	−6.000	0.510	36.225	−29.114	−15.534	12.738	−4.314
0.010	36.000	−24.003	−17.998	12.000	−5.999	0.520	36.234	−29.261	−15.493	12.767	−4.247
0.020	36.000	−24.013	−17.991	12.001	−5.998	0.530	36.243	−29.409	−15.453	12.797	−4.178
0.030	36.001	−24.029	−17.980	12.003	−5.994	0.540	36.252	−29.558	−15.415	12.828	−4.107
0.040	36.001	−24.051	−17.965	12.004	−5.990	0.550	36.262	−29.708	−15.378	12.860	−4.036
0.050	36.002	−24.079	−17.945	12.007	−5.985	0.560	36.271	−29.858	−15.342	12.892	−3.963
0.060	36.003	−24.113	−17.922	12.010	−5.978	0.570	36.281	−30.008	−15.308	12.924	−3.890
0.070	36.004	−24.154	−17.894	12.014	−5.970	0.580	36.291	−30.160	−15.275	12.958	−3.815
0.080	36.005	−24.200	−17.863	12.018	−5.961	0.590	36.302	−30.312	−15.243	12.992	−3.739
0.090	36.007	−24.251	−17.829	12.023	−5.950	0.600	36.312	−30.464	−15.212	13.026	−3.662
0.100	36.009	−24.308	−17.791	12.028	−5.938	0.610	36.323	−30.617	−15.183	13.061	−3.583
0.110	36.010	−24.369	−17.750	12.034	−5.925	0.620	36.333	−30.771	−15.156	13.097	−3.504
0.120	36.012	−24.436	−17.706	12.040	−5.911	0.630	36.344	−30.925	−15.129	13.134	−3.424
0.130	36.014	−24.507	−17.659	12.047	−5.896	0.640	36.355	−31.079	−15.104	13.171	−3.343
0.140	36.017	−24.583	−17.610	12.055	−5.879	0.650	36.367	−31.234	−15.080	13.208	−3.261
0.150	36.019	−24.663	−17.559	12.063	−5.861	0.660	36.378	−31.390	−15.058	13.247	−3.178
0.160	36.022	−24.746	−17.506	12.072	−5.841	0.670	36.390	−31.546	−15.036	13.286	−3.094
0.170	36.025	−24.834	−17.451	12.081	−5.821	0.680	36.402	−31.702	−15.016	13.325	−3.009
0.180	36.028	−24.925	−17.395	12.091	−5.799	0.690	36.414	−31.859	−14.998	13.365	−2.923
0.190	36.031	−25.020	−17.337	12.101	−5.775	0.700	36.426	−32.016	−14.980	13.406	−2.836
0.200	36.034	−25.118	−17.278	12.112	−5.751	0.710	36.439	−32.174	−14.964	13.448	−2.749
0.210	36.038	−25.219	−17.218	12.124	−5.725	0.720	36.451	−32.332	−14.949	13.490	−2.661
0.220	36.042	−25.323	−17.157	12.136	−5.698	0.730	36.464	−32.490	−14.935	13.533	−2.572
0.230	36.045	−25.429	−17.096	12.148	−5.669	0.740	36.477	−32.649	−14.922	13.577	−2.483
0.240	36.049	−25.538	−17.034	12.162	−5.639	0.750	36.490	−32.808	−14.911	13.621	−2.393
0.250	36.054	−25.650	−16.971	12.176	−5.608	0.760	36.504	−32.967	−14.900	13.666	−2.302
0.260	36.058	−25.764	−16.909	12.190	−5.575	0.770	36.517	−33.127	−14.891	13.711	−2.210
0.270	36.063	−25.880	−16.846	12.205	−5.541	0.780	36.531	−33.288	−14.883	13.758	−2.118
0.280	36.067	−25.998	−16.784	12.220	−5.506	0.790	36.545	−33.448	−14.876	13.804	−2.026
0.290	36.072	−26.118	−16.721	12.236	−5.469	0.800	36.559	−33.609	−14.870	13.852	−1.933
0.300	36.077	−26.240	−16.659	12.253	−5.431	0.810	36.574	−33.770	−14.865	13.900	−1.839
0.310	36.083	−26.364	−16.597	12.270	−5.392	0.820	36.588	−33.932	−14.861	13.949	−1.745
0.320	36.088	−26.490	−16.535	12.288	−5.351	0.830	36.603	−34.093	−14.858	13.999	−1.650
0.330	36.094	−26.617	−16.474	12.306	−5.309	0.840	36.618	−34.255	−14.857	14.049	−1.555
0.340	36.099	−26.746	−16.414	12.325	−5.265	0.850	36.633	−34.418	−14.856	14.100	−1.460
0.350	36.105	−26.876	−16.354	12.345	−5.220	0.860	36.649	−34.581	−14.856	14.152	−1.364
0.360	36.112	−27.007	−16.295	12.365	−5.174	0.870	36.664	−34.743	−14.857	14.204	−1.268
0.370	36.118	−27.140	−16.237	12.386	−5.126	0.880	36.680	−34.907	−14.859	14.258	−1.172
0.380	36.124	−27.274	−16.180	12.407	−5.077	0.890	36.696	−35.070	−14.862	14.311	−1.075
0.390	36.131	−27.410	−16.124	12.429	−5.026	0.900	36.712	−35.234	−14.866	14.366	−0.978
0.400	36.138	−27.546	−16.068	12.451	−4.974	0.910	36.728	−35.398	−14.871	14.421	−0.881
0.410	36.145	−27.684	−16.014	12.474	−4.921	0.920	36.745	−35.562	−14.876	14.477	−0.784
0.420	36.152	−27.823	−15.961	12.498	−4.867	0.930	36.761	−35.727	−14.883	14.534	−0.686
0.430	36.159	−27.963	−15.908	12.522	−4.811	0.940	36.778	−35.891	−14.890	14.591	−0.588
0.440	36.167	−28.103	−15.857	12.547	−4.753	0.950	36.796	−36.056	−14.899	14.650	−0.490
0.450	36.175	−28.245	−15.808	12.573	−4.694	0.960	36.813	−36.221	−14.908	14.709	−0.392
0.460	36.183	−28.388	−15.759	12.599	−4.634	0.970	36.830	−36.387	−14.917	14.768	−0.294
0.470	36.191	−28.531	−15.711	12.625	−4.573	0.980	36.848	−36.552	−14.928	14.829	−0.196
0.480	36.199	−28.676	−15.665	12.652	−4.510	0.990	36.866	−36.718	−14.939	14.890	−0.098
0.490	36.207	−28.821	−15.620	12.680	−4.446	1.000	36.884	−36.884	−14.952	14.952	0.000
0.500	36.216	−28.967	−15.576	12.709	−4.381						